Table 1. Experimental settings. CE1

Case name		Climate change and emissions		Emissions	
		Online-PD	Online-NZ	Offline-PD	Offline-NZ
Model		CESM1.2.2	CESM1.2.2	CESM2.2.0	CESM2.2.0
Component		FMOZ	FMOZ	FCSD	FCSD
Physics		CAM4	CAM4	CAM6	CAM6
Chemical mechanism		Tropospheric chemistry with bulk aerosols, MOZART-4		Troposphere/stratosphere chemistry with simplified VBS-SOA, MOZART-TS1	
Dynamics		Free running	Free running	MERRA2 nudging	MERRA2 nudging
Spin-up		2012–2014	2050–2059	2014	2014
Analyzed year		2015–2016	2060–2064	2015	2015
Resolution		1.9° × 2.5° with 26 levels	1.9° × 2.5° with 26 levels	1.9° × 2.5° with 56 levels	1.9° × 2.5° with 56 levels
Emission	in China	2015–DPEC	2060–DPEC	2015–DPEC	2060–DPEC
	outside China	2015–SSP119	2060–SSP119	2015–SSP119	2060–SSP119
CH_4		2015-SSP119	2060-SSP119	2015-SSP119	2060-SSP119
~~Tagging O_3 sources~~		~~TOAST~~		~~O_3S~~	

by 2100 (O'Neill et al., 2014; Rao et al., 2017; Riahi et al., 2017). The emissions inventory includes monthly ~~O_3 precursors, aerosols and their precursors~~ (NO_x, CO, non-methane volatile organic (VOCs), sulfur dioxide (SO_2), ammonia (NH_3), black carbon (BC), organic carbon (OC), dimethyl sulfide (DMS)) and concentrations of greenhouse gases such as CH_4. Biogenic emissions of VOCs are calculated online in CESM using the Model of Emissions of Gases and Aerosols from Nature model (MEGAN; Guenther et al., 2006, 2012). We use emissions for the years 2015 and 2060. Over China, the anthropogenic emissions are replaced by the Ambitious-pollution-Neutral-goals scenario from DPEC (Tong et al., 2020; Cheng et al., 2021). This considers a scenario in which China achieves carbon neutrality by 2060. The DPEC anthropogenic emissions are based on SSP scenarios and MEIC but give anthropogenic emissions at a higher resolution in China, which more accurately characterizes China's emission sources and reflects recent rapid changes in emissions. The total anthropogenic NO emission in China in the Ambitious-pollution-Neutral-goals scenario from DPEC is 1.1 Tg yr^{-1} lower in the present day than in SSP1-1.9 and 1.5 Tg yr^{-1} lower in 2060, but in most regions of eastern China, it is slightly higher. The combined emission distributions for NO_x and its changes in future are shown in Fig. S1 in the Supplement. The total annual mean surface emissions of key pollutants from anthropogenic (ANT), biomass burning (BB) and biogenic (BIO) sources for the present day (2015) and future net zero (2060) over the globe and in east Asia are listed in Table 2.

The global anthropogenic emissions of all O_3 precursors are significantly reduced in the net-zero scenario. Due to strict control policies on pollutant emissions and changes in technology and behavior, global anthropogenic NO emissions decrease from 87 Tg yr^{-1} in the present day to 19 Tg yr^{-1} in 2060, and total anthropogenic VOC emissions decrease from 125 to 28 Tg yr^{-1}. Biomass burning emissions also decrease slightly. Natural NO soil emission, VOC biogenic emission and CO ocean emission are assumed not to change in this study as changes in land use are relatively small. Anthropogenic emissions over east Asia account for more than 35 % of the global total, with biomass combustion emissions accounting for a smaller proportion at ∼ 10 % and with natural emissions of NO, VOCs and CO accounting for ∼ 20 %. The decrease of anthropogenic emissions over east Asia (about 80 % for NO) is greater than the global average of > 70 %, which may be due to the high present-day emissions over the region, especially in eastern China. The global CH_4 concentration decreases from the current 1831 ppbv to 1312 ppbv due to the lower global CH_4 emissions under net zero.

2.3 Tagging of ozone

In this study, we use the Tropospheric Ozone Attribution of Sources with Tagging (TOAST) ozone methodology in CESM1.2.2 previously described by Butler et al. (2018, 2020) to perform separate source attributions of ground-level O_3 to NO_x. The parameterizations based on the work of Butler et al. (2018, 2020) include tagging the biogenic, biomass burning and anthropogenic emissions of NO_x or VOCs by their geographical source regions. This tagging methodology allows us to examine the seasonal cycle of the surface O_3 attribution in receptor regions using ~~those~~ CE2 defined in the Hemispheric Transport of Air Pollutants Phase 2 (HTAP2, Janssens-Maenhout et al., 2015; Koffi et al., 2016). We consider 16 sources, including 11 geographical source regions for anthropogenic NO_x emission, shown in Table 3 and Fig. 1; NO_x emissions from biogenic sources (BIO); biomass burning (BB); aircraft (AIR) and lightning (LIG); and O_3 originating in the stratosphere (STR).

2.4 Measurement data

To evaluate tropospheric column O_3 in the model simulations, we use a present-day satellite dataset of tropospheric column O_3 which was derived by combining retrievals from the Aura Ozone Monitoring Instrument (OMI) and Microwave Limb Sounder (MLS) observations (https://acd-ext.gsfc.nasa.gov/Data_services/cloud_slice/, last access: TS8).

Table 4. Global tropospheric O_3 burden (Tg) and budget terms (Tg yr^{-1}) in chemical transport models. TS11

Models	Prod	Loss	NetChem	Residual	DryDep	Burden (O_3/O_3S)	Lifetime (days)	Reference
Globe				STE				
~~33~~	~~3948 ± 761~~	~~3745 ± 554~~	~~245 ± 346~~	~~636 ± 273~~	~~902 ± 255~~	~~307 ± 38~~	~~21–25~~	~~Wild (2007)~~
17	4465 ± 514	4114 ± 409	396 ± 247	529 ± 105	949 ± 222	314 ± 33	~~22 ± 2~~	~~Stevenson et al. (2006)~~
~~15~~	5110 ± 606	4668 ± 727	442 ± 309	552 ± 168	1003 ± 200	344 ± 39	22 ± 2	~~Young et al. (2013)~~
PI	2549	2437	112	415	528	241	29	Griffiths et al. (2021)
PD	4510	3948	562	284	846	337	26	
PD	**5038**	**4641**	**397**	**595**	**992**	**316/69**	**20**	**This study**
NZ	**3392**	**3311**	**81**	**626**	**707**	**247/77**	**22**	**This study**
East Asia				Transport				
PD	**682**	**455**	**227**	**−89**	**138**	**25/5**	**15**	**This study**
NZ	**430**	**293**	**137**	**−38**	**99**	**19/6**	**17**	**This study**

Prod is for chemical production, Loss is for chemical loss, Prod-Loss is for net chemical production (NetChem), and DryDep is for dry deposition; Residual is the term balance by Residual = Loss-Prod + DryDep. Units of Prod, Loss, NetChem, Residual and DryDep are in Tg(O_3) yr^{-1}, Burden is in Tg(O_3), and Lifetime is in days. The climatological pressure tropopause is used. PD is the online present-day experiment simulation. NZ is the online net-zero experiment simulation. The results of Griffiths et al. (2021) are the average of four models (UKESM1, CESM2-WACCM, GFDL-ESM4, MRI-ESM2-0), and PD is the average from 1995 to 2004, while PI (pre-industrial) is the average from 1850 to 1859.

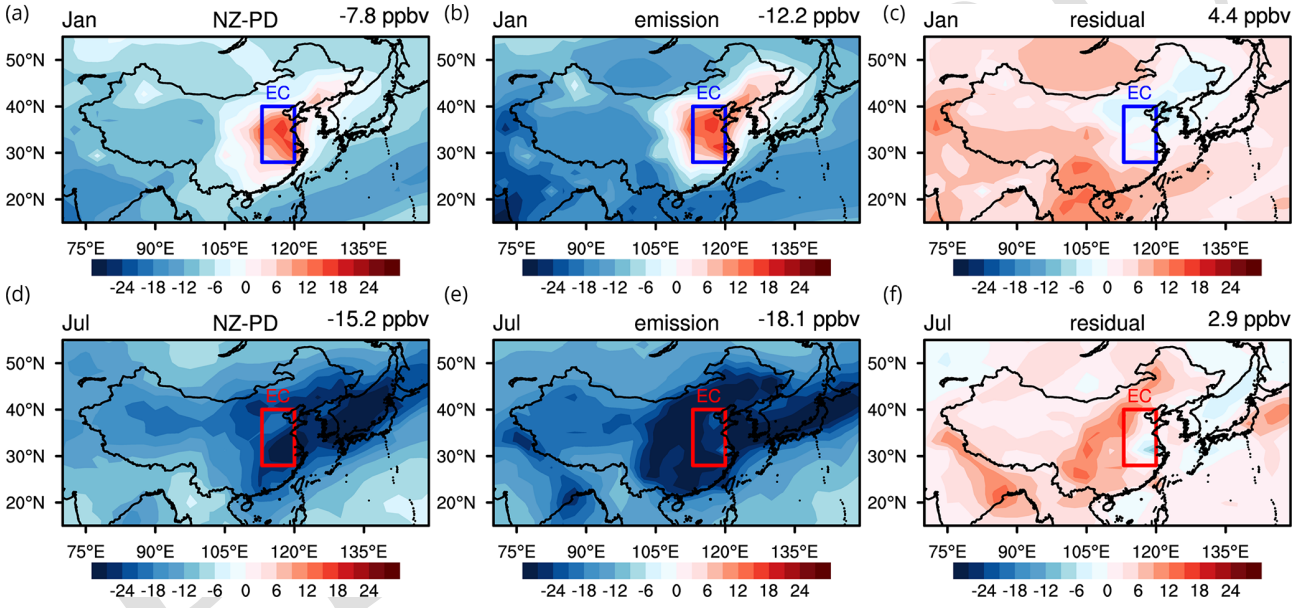

Figure 4. Changes in surface O_3 mixing ratio (ppbv) over China in January and July between present day and net zero (online-NZ minus online-PD; **a, d**) and changes due to emissions (offline-NZ minus offline-PD; **b, e**) and the residual (left minus middle panel; **c, f**). The values in the right corner of each panel are the region means over east Asia (15–55° N, 70–149° E). The frame is the region of eastern China (EC, 28–40° N, 113–120° E).

in winter and a greater reduction of 16.2 ppbv in summer. Turnock et al. (2019) estimated an annual mean reduction of 8 ppbv in 2050 under the SSP1-1.9 pathway, slightly less than we find here. However, we have used the more stringent DPEC Ambitious-pollution-Neutral-goals emission scenario for China rather than the standard SSP1-1.9 pathway, and we note that anthropogenic NO emissions in China are 1.5 Tg (NO) yr^{-1} lower in this scenario than those in SSP1-1.9. Surface O_3 over eastern China and South Korea increases in winter in these scenarios, driven by the reduction in emissions (left and middle panels). This increase in surface O_3 is caused by a weakening of titration under lower regional NO emissions in the future. The influence of climate change on surface O_3 is relatively weak and leads to an increase in surface O_3 in most parts of east Asia (right panels). This is partly due to enhanced vertical circulation leading to an increased contribution from stratospheric O_3 (Akritidis et al., 2019; shown in Fig. S4) and the photochemical change under warmer climate (Zanis et al., 2022). Xu et al. (2022) also showed that emission reduction is far more effective than climate change in improving air quality ($PM_{2.5}$ and O_3) over east Asia under a carbon-neutral reduction pathway. Here, we will use tagging simulations to quantify the contributions of different sources to surface O_3 changes over east Asia,

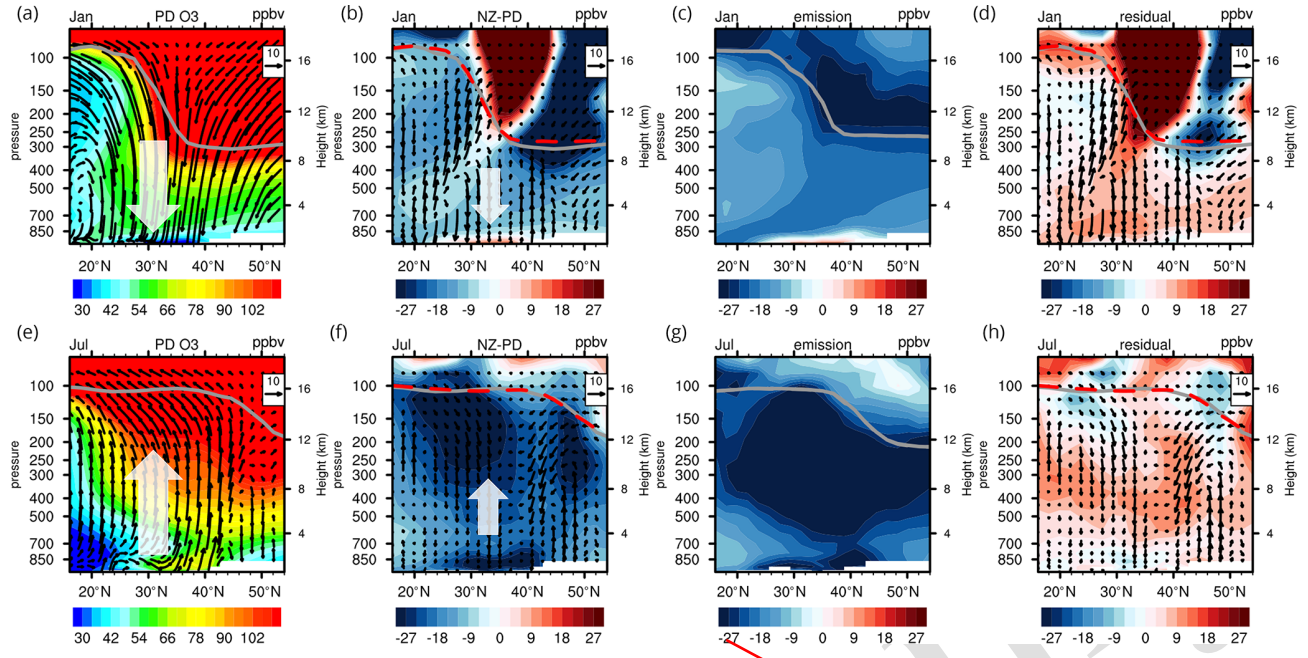

Figure 5. Zonal mean O_3 cross-section (ppbv) and wind speed (vectors, v: m s^{-1}, w: *(−500) pa s^{-1}) over eastern China (longitudes 111–122° E) in January and July under present-day conditions (online-PD, **a, d**), the changes in O_3 and wind speed **(b, f)** and changes due to emissions **(c, g)**, and the residual (second panels minus third panels; **d, h**). Grey lines show the tropopause location under present-day conditions; the dashed red lines show the tropopause location under net zero.

We would like change the up arrow to down arrow. Could we replace the Figure 5? The new figure is in the email attachments.

Explanation:
We had marked the wrong direction of the arrow in panel f. The anomaly wind is downdraft.It will be perfect after the correction.

especially over eastern China where surface O_3 increases in winter and decreases in summer.

It can be seen from the vertical distribution of O_3 and circulation (shown in the first panels of Fig. 5) that the O_3 concentration increases with altitude under present-day conditions. At the same altitude, the O_3 concentration is higher in middle and high latitudes than in low latitudes. In winter, there is a strong net descent of air over eastern China (30–40° N), which weakens in spring and turns to updraft in summer. These may be due to the weakened Brewer–Dobson circulation and strengthened convection (Butchart, 2014; Wild and Akimoto, 2001). As shown in the second panels of Fig. 5, there is a net decrease in tropospheric O_3 in future, with an increase only seen near 30° N very close to the surface. In summer, the reduction in tropospheric O_3 is greatest, especially near the tropopause where it exceeds 30 ppbv. In addition, due to the temperature increase and circulation enhancement in the future, the tropopause height increases, especially in the mid-latitude region in winter, where the increase is about 7 hPa. As seen from the third panels of Fig. 5, the reduction in emissions from aircraft (NO emissions in Fig. S1) leads to a reduction in O_3 production, and the O_3 concentration near the tropopause decreases substantially in the future. However, other factors such as climate change (the fourth panel in Fig. 5) lead to increases in tropospheric O_3 by 2060.

5

Surf… east
Asia… hes a
max… n Au-
gust… con-
centration of surface O_3 is lower throughout the year, and while the peak is still in March, the mixing ratio drops to 43 ppbv. The decrease is greatest in July at 16 ppbv, which reflects weaker chemical production in summertime under lower future emissions (Fig. 6e). In contrast, surface O_3 over eastern China is highest (71 ppbv) in July and lowest (21 ppbv) in December under present-day conditions (Fig. 6b). Under net zero, surface O_3 increases in winter and decreases in summer, and the peak shifts from July to May due to the changes in O_3 precursor emissions (Bowman et al., ~~2021~~TS12). This shifts the seasonal peak from summer towards spring, when it is more greatly influenced by stratosphere–troposphere exchange. The decrease is highest in July, as seen over the wider east Asian region, but it is twice as large at 34 ppbv, reflecting the stronger present-day emissions over eastern China. There is a substantial increase in O_3 in January of 12 ppbv, reflecting reduced titration by NO. The concentration of surface NO_x decreases by more than 60 % and by an even larger factor in winter (∼ 90 %, 14 ppbv), and its seasonal variation is reduced, which accounts for the reduction in anthropogenic emissions